ADVANCED FUNCTIONAL MATERIALS
www.afm-journal.de

Dual Coordination of Ti and Pb Using Bilinkable Ligands Improves Perovskite Solar Cell Performance and Stability

Furui Tan, Makhsud I. Saidaminov, Hairen Tan, James Z. Fan, Yuhang Wang, Shizhong Yue, Xiaotian Wang, Zhitao Shen, Shengjun Li, Junhwan Kim, Yueyue Gao, Gentian Yue, Rong Liu, Ziru Huang, Chen Dong, Xiaodong Hu, Weifeng Zhang, Zhijie Wang,* Shengchun Qu, Zhanguo Wang, and Edward H. Sargent**

Charge recombination due to interfacial defects is an important source of loss in perovskite solar cells. Here, a two-sided passivation strategy is implemented by incorporating a bilinker molecule, thiophene-based carboxylic acid (TCA), which passivates defects on both the perovskite side and the TiO_2 side of the electron-extracting heterojunction in perovskite solar cells. Density functional theory and ultrafast charge dynamics reveal a 50% reduction in charge recombination at this interface. Perovskite solar cells made using TCA-passivated heterojunctions achieve a power conversion efficiency of 21.2% compared to 19.8% for control cells. The TCA-containing cells retain 96% of initial efficiency following 50 h of UV-filtered MPP testing.

1. Introduction

Organic–inorganic hybrid perovskite solar cells recently surpassed 25% certified power conversion efficiency (PCE).[1–3] High performance has been achieved in part through reducing charge recombination losses at interfaces,[4–6] especially at the electron-extracting interface;[7,8] this is especially important in mesoporous structures that produce large interfacial areas.[9,10] Reported interface engineering methods typically target A-site passivation in ABX_3 perovskites through the formation of weak van der Waals bonds between perovskite and functional groups such as $-NH_2$, $-CN$, fullerene derivatives ($-C_{60}$), and aromatic groups.[11–14] However, the volatile nature of organohalide salts (such as methylammonium iodide (MAI)) in perovskites results in the formation of undercoordinated B-site cations (Pb^{2+}) that act as electron traps.[15,16] Passivation of such defects using thiourea and anionic acids has been an important step,[9,17–19] but the resultant thick molecular layer acts as an energy barrier. In addition, prior passivation approaches have targeted only one surface of the two contact materials, most typically the perovskite side. This leaves the other side with a higher density of defects.[10,20]

Here, a double contact passivation strategy was developed by using a functional molecule, 3-thiophenecarboxylic acid (TCA),

Dr. F. Tan, Dr. Z. Shen, Dr. S. Li, Dr. Y. Gao, Dr. G. Yue, Dr. R. Liu, Dr. C. Dong, X. Hu, Prof. W. Zhang
Key Laboratory of Photovoltaic Materials
Henan University
Kaifeng, Henan 475004, China
E-mail: wfzhang@henu.edu.cn

Dr. F. Tan, Dr. M. I. Saidaminov,[+] J. Z. Fan, Dr. Y. Wang, Dr. J. Kim, Z. Huang, Prof. E. H. Sargent
Department of Electrical and Computer Engineering
University of Toronto
Toronto, Ontario M5S 3G4, Canada
E-mail: ted.sargent@utoronto.ca

Prof. H. Tan
National Laboratory of Solid State Microstructures
Jiangsu Key Laboratory of Artificial Functional Materials
College of Engineering and Applied Sciences
Nanjing University
Nanjing 210093, China

The ORCID identification number(s) for the author(s) of this article can be found under https://doi.org/10.1002/adfm.202005155.

[+]Present address: Department of Chemistry, Department of Electrical and Computer Engineering, Centre for Advanced Materials and Related Technologies (CAMTEC), University of Victoria, Victoria, BC V8W 2Y2, Canada

S. Yue, Prof. Z. Wang, Prof. S. Qu, Prof. Z. Wang
Key Laboratory of Semiconductor Materials Science
Beijing Key Laboratory of Low Dimensional Semiconductor Materials and Devices
Institute of Semiconductors
Chinese Academy of Sciences
Beijing 100083, China
E-mail: wangzj@semi.ac.cn

X. Wang
School of Civil Engineering
Hefei University of Technology
Hefei 230009, China

Prof. J. Kim
Photo-electronic Hybrids Research Center
Korea Institute of Science and Technology (KIST)
Seoul 02792, Korea

DOI: 10.1002/adfm.202005155

a short-chained (≈0.332 nm) bilinkable (carboxyl and thioether) molecule with a directed dipole to passivate both the ETL and the perovskite at the interface. On TiO_2 nanorod array (NR) ETLs that possess well-aligned electron transport channels, but suffer from a high density of surface oxygen vacancies,[21,22] the TCA increased the PCE from 19.8% for control devices to 21.2% for TCA-passivated devices. Operating stability characterization shows that TCA-incorporating perovskite solar cells retained 92% of their initial PCE following 12 h at MPP under full solar illumination; and 96% of their initial PCE following 50 h of UV-filtered AM1.5 illumination.

2. Results and Discussion

The solar cells architecture for this work is as: FTO/TiO_2 dense layer/TiO_2 NRs (with or without TCA)/perovksite ($Cs_{0.05}FA_{0.9}MA_{0.05}PbI_{2.55}Br_{0.45}$)/Spiro-OMeTAD/Au. TiO_2 NRs with tunable rod lengths were synthesized via the hydrolysis of titanium butoxide on a compact TiO_2 seed layer (Figure S1, Supporting Information). The resultant substrates were treated with TCA in a water:ethanol mixture.

The nature of the TCA:TiO_2 interaction was studied using X-ray photoelectron spectroscopy (XPS) and Fourier transform infrared (FTIR) spectroscopy. XPS shows that the O1s signal for the TCA:TiO_2 sample exhibits a pronounced shoulder at 531.9 eV (**Figure 1**b, Figure S2 and Table S1, Supporting Information) compared to that of TiO_2 (Figure 1a), associated with the coordination of carboxyl group to Ti.[23,24] FTIR spectra of TCA-TiO_2 show a broad absorption band at 550–750 cm^{-1} which is indicative of the O-Ti vibration (650–750 cm^{-1}) in TiO_2 and the bending vibration of Ti—O—C=O in TCA-TiO_2 (Figure 1c and Figure S3, Supporting Information). The TCA-TiO_2 sample also exhibits a C=O stretch vibration at 1740 cm^{-1} from TCA. The broadened O—H vibrational signal at 3450 cm^{-1} is assigned to the combination of signals from the carboxylate —OH from TCA and adsorbed H_2O on TiO_2. These results support the view that the carboxyl group of TCA is anchored to the TiO_2.

Electron paramagnetic resonance (EPR) spectroscopy was used to study oxygen vacancies (Figure 1d). The strong signal near 3380 Gs (corresponding to a paramagnetic factor g of 2.01) indicates a high density of oxygen vacancies in bare TiO_2 samples.[25,26] In comparison, a reduced peak intensity was found for TCA-TiO_2. The reduction in oxygen vacancy density lies in the single-crystal nature of TiO_2 nanorods: it ensures most oxygen vacancies are on the surface, and offers the benefit that this region is accessible to surface passivation (Figure S4, Supporting Information).

It is posited that TCA molecules could reduce trap states at the perovskite/ETL interface by electrically bridging the two materials (**Figure 2**a). Surface photovoltage (SPV), a technique correlated with defect-induced surface band bending, [27,28] was characterized to obtain further insight. The SPV spectra of TiO_2 showed a peak at 371 nm with a notable shoulder at 400 nm (Figure 2b and Figure S5, Supporting Information). The latter is assigned to delocalization and separation of trapped charges from surface states at 0.3 (1240/371–1240/400) eV below the conduction band minimum (CBM).[29,30] The shoulder response was reduced for TCA-TiO_2 samples, indicating a lower density of surface states.

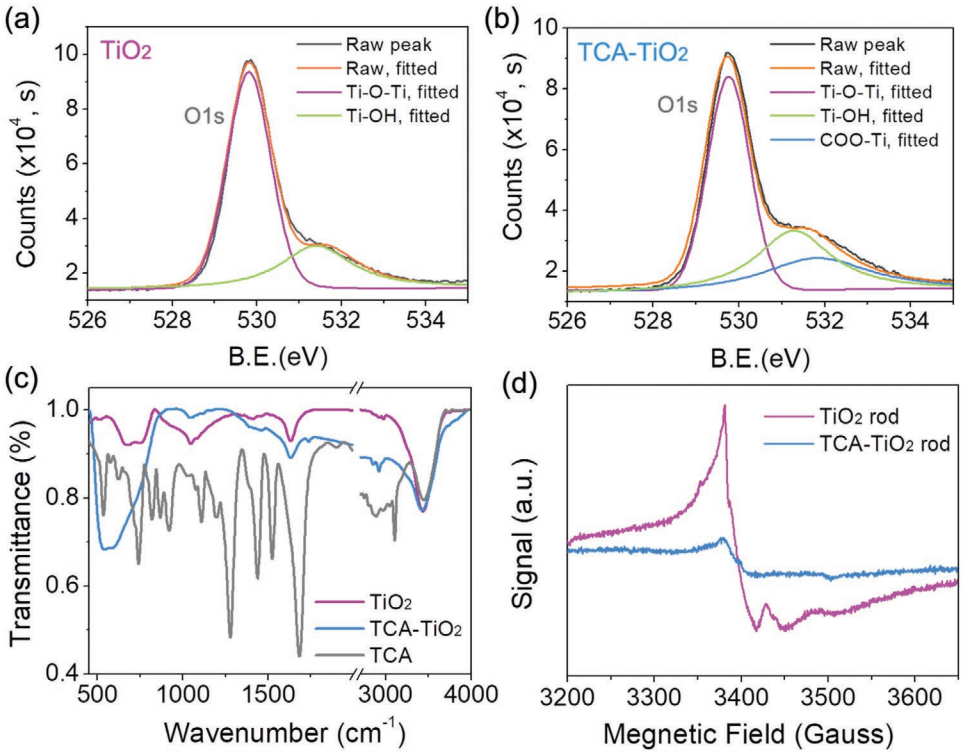

Figure 1. O 1s X-ray photoelectron spectra (XPS) of a) TiO_2 and b) TCA modified TiO_2 nanorod arrays. c) Fourier transform infrared spectroscopy (FTIR) of TiO_2 and TCA-TiO_2 powder. d) Electron paramagnetic resonance (EPR) spectra of TiO_2 rods versus TCA-TiO_2 rods.

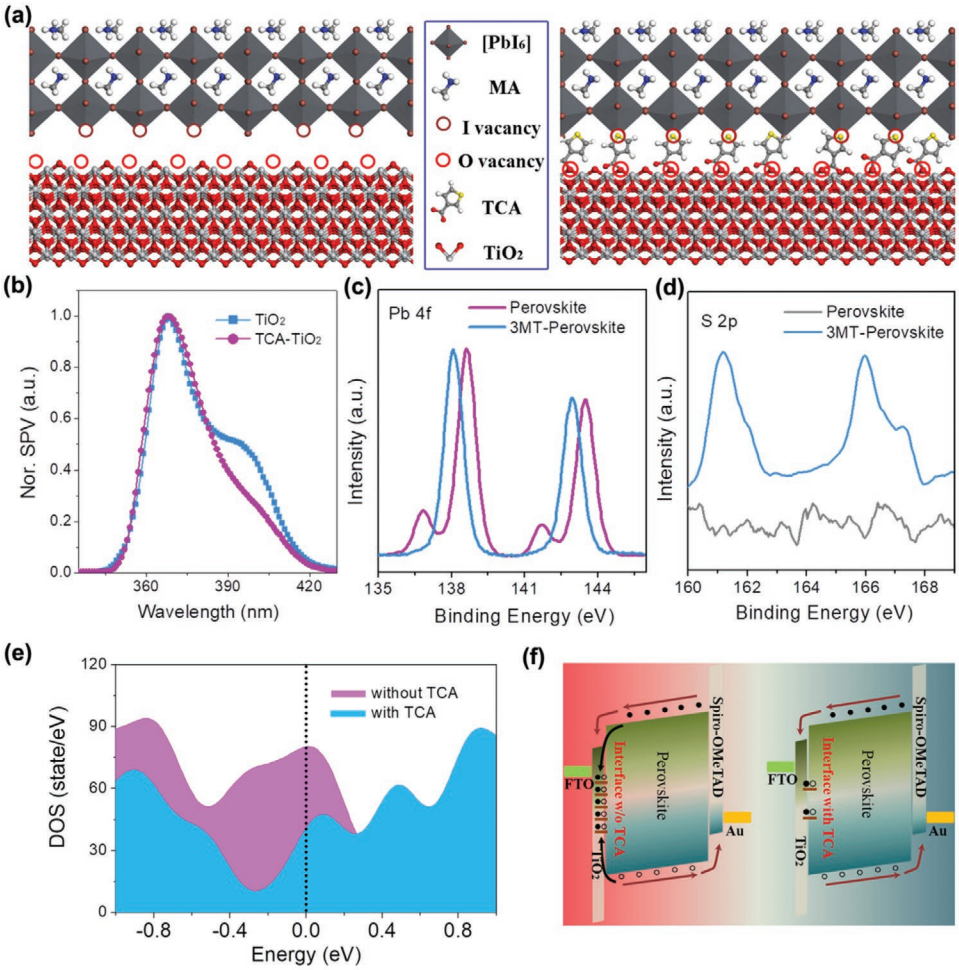

Figure 2. a) Schematic of perovskite/TiO_2 interface with and without TCA. The defect-induced trap states at the interface cause charge recombination in the control cells, a process that is slowed in the cells with TCA. b) Normalized surface photovoltage (SPV) spectra of TiO_2 and TCA-TiO_2 nanorods. c) XPS Pb 4f and d) S 2p signals of perovskite and 3MT modified perovskite. e) Density of states at the perovskite/TiO_2 interface with and without TCA. f) Energy diagram and charge transfer processes in the studied solar cells.

The volatile nature of organohalide salt leads to halide deficiency, leaving perovskite surfaces with under-coordinated Pb.[15,16] The Pb4f XPS of control perovskite film showed two satellite peaks that were assigned to the uncoordinated Pb (Figure 2c).[17,31,32] This class of defects are known as nonradiative trap states near the CBM.[33] The perovskite film treated with a monolinkable 3-methylthiophene (3MT) ligand showed S-Pb interaction signal at low binding energies along with C−S−C S2p peaks (Figure 2d).[34] 3MT was selected herein because it is monolinkable through the thiophene functional group that passivates the perovskite surface. As a result, the Pb4f peaks shifted toward low binding energy due to improved Pb coordination,[35] and the two satellite peaks disappeared. Similarly, S-Pb-I coordination has been associated with advances in PbS quantum dot solar cell performance.[36,37] Density functional theory (DFT) was used to study the density of states (DOS) at the perovskite:TiO_2 interface. Calculated trap densities for TCA-treated films are 1.7 ± 0.3 times lower than untreated perovskite films. (Figure 2e). Therefore, the TCA linkage on perovskite reduces nonradiative recombination via passivation (Figure 2f).

Photoluminescence (PL) measurements were used to characterize the passivation properties of the TCA treatment. The PL intensity was enhanced upon direct treatment of perovskites with TCA, an effect also observed in perovskite:3MT films (**Figure 3**a). Time-resolved PL (TRPL) showed a longer minority carrier lifetime for the ligand-modified perovskite films (183 ns and 215 ns for TCA and 3MT, respectively) compared to the bare sample (125 ns) (Figure 3b); this indicates lower nonradiative recombination losses in treated films.[38,39]

TiO_2:perovskite heterojunction energy level alignment was studied using ultraviolet photoelectron spectroscopy (UPS) (Figure 3c, Table S2 and Figure S6, Supporting Information). The conduction band (CB) of surface TCA-TiO_2 upshifted by 110 mV (ΔV in Figure 3d) compared to bare TiO_2. The surface band bending of TiO_2 nanorod can be influenced by several factors such as nanorod morphology, molecule/metal decoration, surface defects and dipole interactions.[40–43] In our case, TCA adsorption on Ti dangling bonds through carboxyl groups decreases surface trap states and downshifts the surface energy band of TiO_2. However, the interfacial dipole (estimated to be ≈1.71 D by DFT calculation) induced by the coordinative TCA

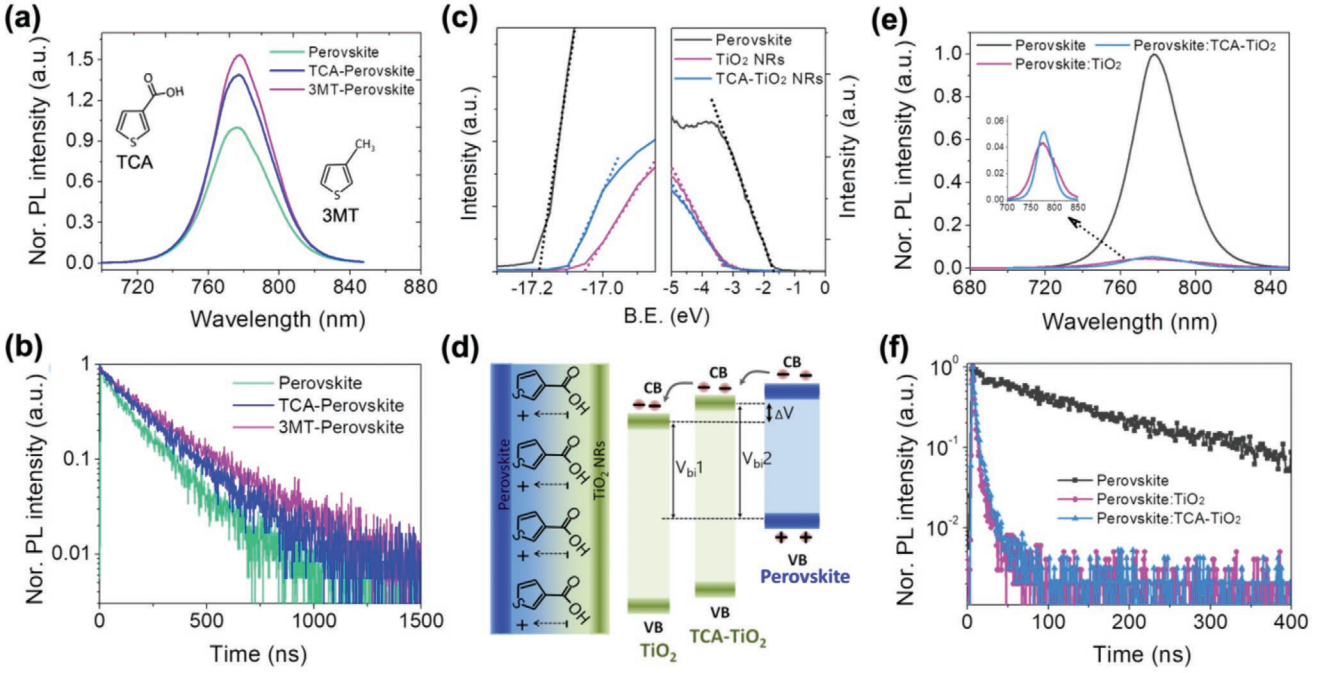

Figure 3. a) Steady-state and b) transient photoluminescence (PL) properties of perovskite films treated using different molecules. c) Ultraviolet photoelectron spectra (UPS) of TiO_2, TCA-TiO_2 NRs, and CsMAFA perovskite films. d) Energy level alignment of TiO_2/perovskite and TCA-TiO_2/perovskite heterojunction. The left panel shows the interfacial TCA modification-induced interface dipole. V_{bi} stands for the built-in field of the heterojunction. ΔV represents the TiO_2's CB shift due to TCA modification. e) Steady-state and f) transient PL of perovskite films on different TiO_2 substrates.

tends to repel surface electrons in TiO_2 because of the dipole vector pointing from perovskite to TiO_2. This elevates the surface energy band of TiO_2.[19] The final surface band bending is a result of balance between these factors.[44] Although the band offset between the CB of TiO_2 and perovskite films was reduced after TCA modification, efficient electron transfer was still retained, as demonstrated from steady state and time resolved PL measurements on heterojunctions (Figure 3e,f). Physically, photogenerated electrons diffuse from the high-Fermi-level perovskite to the low-Fermi-level ETL; this causes a reduction in radiative recombination.[45]

To explore the effect of TCA on photovoltaic performance, hybrid perovskite solar cells were fabricated based on mixed-halide triple cation ($Cs_{0.05}MA_{0.05}FA_{0.9}PbI_{3x}Br_{3(1-x)}$).[46,47] The perovskite films on TiO_2 and TCA-TiO_2 show similar grain sizes and morphology (Figures S7 and S8, Supporting Information). Therefore, the TCA modification does not change the active layer structure of the perovskite, The statistical performance from 80 devices showed that the PCE was improved from (19.3 ± 0.4)% to (20.5 ± 0.4)% following TCA modification (**Figure 4**a). The best cells employing control TiO_2 NRs showed a PCE of 19.8% with a hysteresis index (HI, $(Eff_{rev} - Eff_{for})/Eff_{rev}$) of 2.5% (Figure 4b). When the TCA-TiO_2 ETL was used, the champion efficiency increased to 21.2% and the HI value dropped to 0.4%. We attribute the enhancement in V_{oc} (ΔV = 11 mV) and FF (ΔFF = 3.7%) to suppressed nonradiative recombination in TCA-TiO_2 solar cells compared to control TiO_2 solar cells with similar light absorption (Figure S6, Supporting Information). The increased J_{sc} for TCA-TiO_2 devices can be attributed to enhanced charge collection. External quantum efficiency (EQE) spectra (Figure S9, Supporting Information) show that TCA-TiO_2 devices generated higher EQE across the entire spectrum, consistent with the higher J_{sc} (Figure 4b).

The operational stability of the two solar cells was examined under maximum power point (MPP) tracking (Figure 4c). TCA-TiO_2 devices shows a gradual decrease in efficiency from 21% to 19.4% following 12 h of constant AM1.5 light exposure; while that of control TiO_2 devices decreased from 19.5% to 16.7%. When a 420 nm cutoff UV was used,[48] the TCA-TiO_2 and the control cells retained 96% and 91% of their initial efficiencies, respectively, following 50 h of MPP tracking (Figure S10, Supporting Information). This stability tendency is comparable to the literature reports in the given time window.[7,47] It is known that TiO_2 defects have led to UV-photocatalytic degradation;[49,50] and defects in the perovskite itself have also been studied as a source of degradation.[17]

A series of optoelectronic measurements were performed to investigate the mechanism behind the observed improvements. Electrochemical impedance spectra (EIS) were collected at different bias voltages from 0 V to 1.1 V at frequencies ranging from 1 MHz to 1 KHz (**Figure 5**a, Figure S11 and Table S3, Supporting Information). The diameter of Nyquist plot at medium frequencies (100 KHz to 1 KHz) represents charge transfer recombination resistance (R_{ct}).[51,52] The R_{ct} is larger in TCA-TiO_2 cells than that in the control devices, indicating a suppressed charge recombination at the TCA-modified interface. A relatively small reverse current density in the dark suggests lower current leakage loss for TCA-TiO_2 devices compared to controls (Figure S12, Supporting Information). Using pump fluence-dependent PL studies (Figure 5b),[53] we found that the trap saturation threshold (P_{st}^{trap}) is 2.7 and 1.9 μJ cm^{-2} for the control and TCA modified perovskite films, respectively.

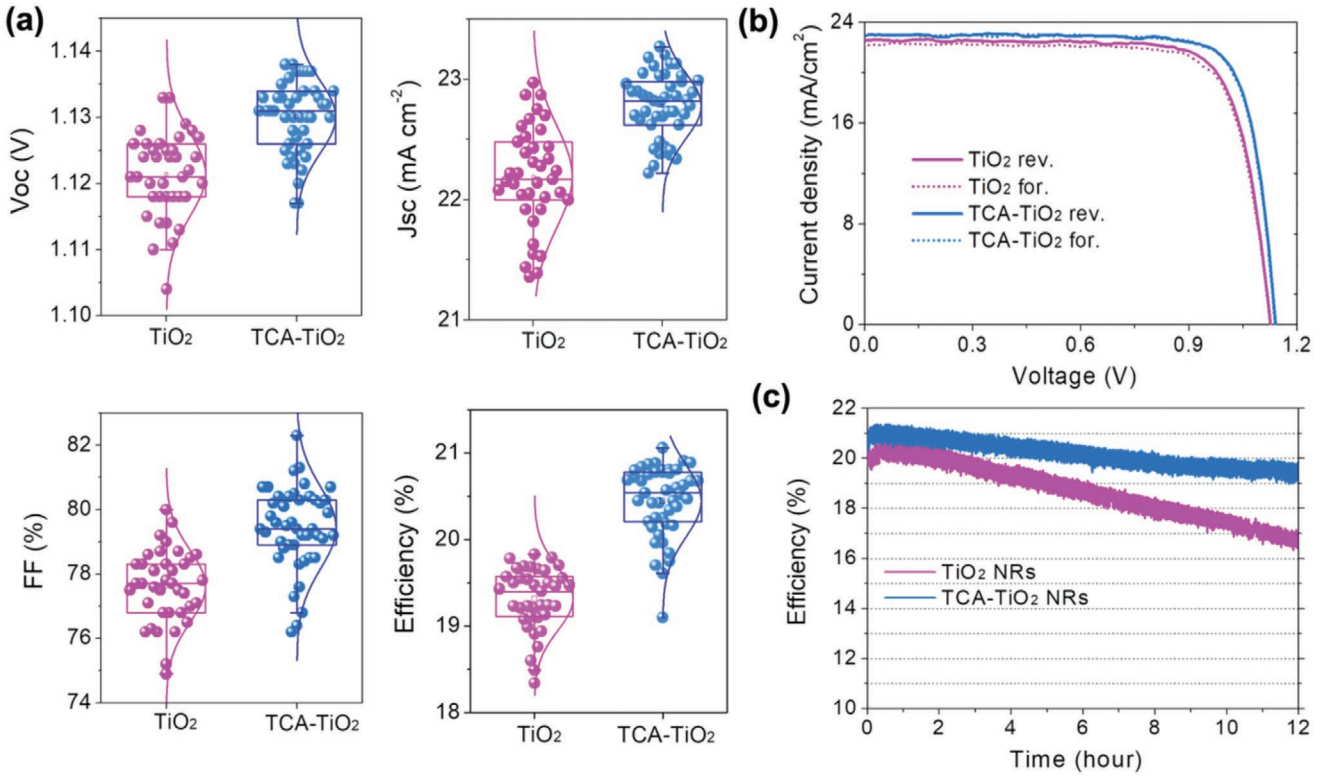

Figure 4. a) Performance statistics of solar cells made with a triple cation perovskite absorber. b) JV curve of champion cells with and without TCA modification. c) Stability of solar cells under maximum power point (MPP) tracking with AM 1.5 illumination. The cells were tested under N_2 and without encapsulation.

Space-charge-limited current (SCLC) analysis revealed that the trap density of perovskite film is reduced from $(3.1 \pm 0.1) \times 10^{15}$ to $(1.9 \pm 0.2) \times 10^{15}$ cm^{-3} after TCA incorporation (Figure S13, Supporting Information).[39,54] We conclude that the TCA bilinkable bridge at the interface contributed to a reduced interfacial trap density and promoted enhanced charge transfer with suppressed nonradiative recombination loss.

Scanning Kelvin probe microscopy (SKPM) showed that perovskite films on TCA-TiO_2 generate an average surface potential of 159 ± 7 mV, larger than that of 102 ± 6 mV for the control sample (Figure 5c). As TiO_2 extracts photogenerated electrons, the observed increase in surface potential is likely due to an increase of hole concentration on the surface of perovskite.[28] Time-resolved SPV showed a life time of 70 µs for the TCA-modified cells, 2 × larger than that for the control devices (Figure 5d). These results demonstrate that the interfacial TCA bilinkable coordination allows for effective defects passivation and carrier transfer in perovskite solar cells.

To understand the necessity of the bilinkable nature, alternative solar cells were fabricated using monolinkable molecules having structure similarity with TCA: 3MT and benzoic acid (BA) (Figure S14a, Supporting Information). 3MT has the thioether terminal group for perovskite side passivation, while BA has the carboxyl terminal group for TiO_2 anchoring. Statistics on photovoltaic performance indicate that neither of the two monodentate molecules achieves the same performance as the bilinkable TCA (Figures S14 and S15 and Table S4, Supporting Information).

3. Conclusions

In conclusion, we explored interfacial modification using a bilinkable TCA molecule that coordinates both Ti and Pb at perovskite/TiO_2 NR interfaces. TCA, as a dipole, facilitates charge transfer at this interface and suppresses charge nonradiative recombination. This TCA-aided interface passivation improved the performance of solar cells from 19.8% to 21.2%. TCA incorporation also improved the stability of solar cells under full and also UV-filtered illumination.

4. Experimental Section

Synthesis of TiO_2 NRs: iO_2 NRs were prepared according to a previous method.[55] Various rod lengths were achieved through tuning the hydrothermal reaction time. Samples were obtained using reaction times of 1.5, 2.0, and 3.0 h. The TiO_2 NR substrates were washed with deionized water, ethanol, and acetone for 10 min respectively, and then dried using N_2. The substrates were annealed at 450 °C for 60 min.

TCA Modification on TiO_2 NRs: TCA powder (99%, Sigma-Aldrich) was dissolved in water: ethanol (1:1 in volume ratio) solvent mixture and the solution was heated to 60 °C. The NR substrates were immersed in the solution and aged for 12 h during which the temperature was kept at 50–60 °C. Then, the substrates were taken out and washed using ethanol. The TCA-treated NRs substrates were dried at 60 °C in vacuum and then immediately transferred into a N_2 filled glove box.

Fabrication of Perovskite Solar Cells: In N_2 filled glove box, a $Cs_{0.05}FA_{0.9}MA_{0.05}PbI_{2.85}Br_{0.15}$ solution was prepared by dissolving the precursors in *N*,*N*-dimethylformamide:dimethylsulfoxide (DMF:DMSO)

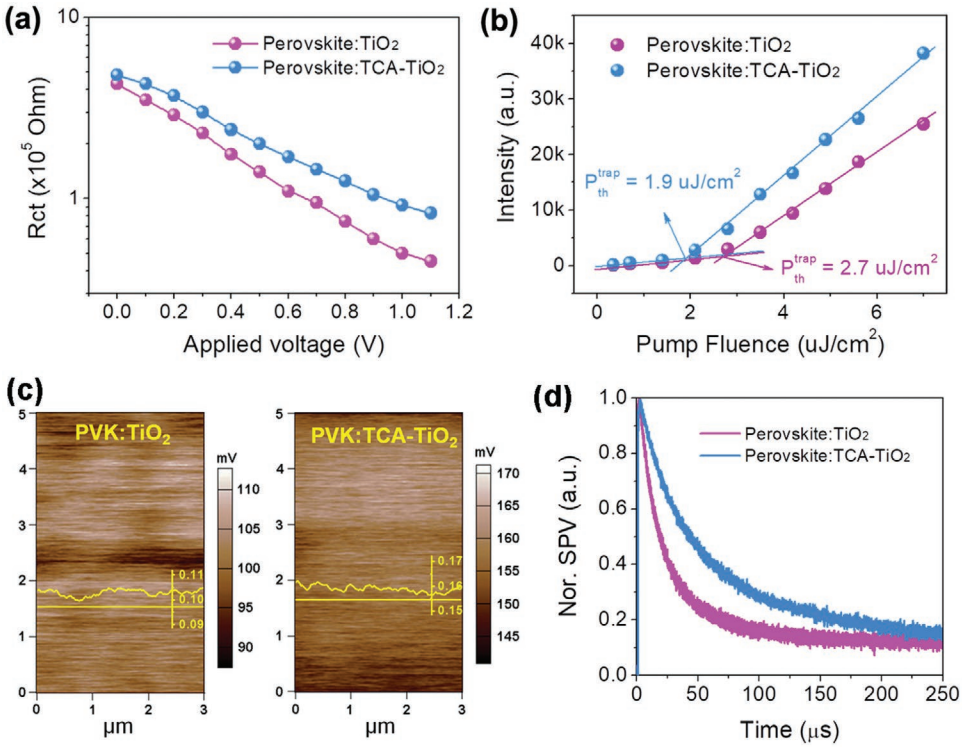

Figure 5. a) Charge transfer recombination resistance (R_{ct}) as a function of applied bias. b) Pump fluence-dependence of PL of perovskite:TiO_2 substrates with and without TCA. c) Scanning Kelvin probe microscope (KPM) images of perovskite films on TiO_2 and TCA-TiO_2 surfaces. The yellow curve shows the KPM values along the yellow line. d) Normalized transient surface photovoltage spectra of solar cells.

mixed solvent with a volume ratio of 4:1 at 70 °C and stirring overnight. The transparent yellowish solution was filtered with 0.45 um poly(vinylidene fluoride) (PVDF) filter. Before perovskite deposition, the NR (with and without TCA modification) substrates were preheated at 60 °C. The perovskite solution was deposited onto NR substrates, waited 30 s and then spin-coated using a two-step spin-coating procedure (1000 rpm for 10 s and 6000 rpm for 30 s). 200 ul chlorobenzene were deposited at 20s from the beginning of the second spin-coating stage. The perovskite films were annealed at 100 °C for 30 min. The hole-transport layer (Spiro-OMeTAD) was deposited on perovskite films by spin-coating the solution at 4000 rpm (containing 65 mg mL^{-1} Spiro-OMeTAD, 70 $\mu L mL^{-1}$ bis(trifluoromethane)sulfonimide lithium salt (170 mg mL^{-1} in acetonitrile), 20 $\mu L mL^{-1}$ tert-butylpyridine). Finally, 120 nm Au was deposited on top of Spiro-OMeTAD by electron-beam evaporation under a vacuum of 8×10^{-7} Torr.

Solar Cell Characterization: Current density–voltage (*J–V*) curves were obtained using a Keithley 2400 current–voltage meter with the device under AM1.5G illumination (Newport, Class A). The scan rate was fixed at 50 mV s^{-1} from 1.2 to –0.1 V with 10 mV voltage steps. The stabilized power output was obtained by setting the bias voltage to the initial V_{MPP} that was determined from the *J–V* curve. The active area (0.049 cm^2) was determined using an aperture shade mask. EQE measurements were performed using a Newport system (QuantX-300) calibrated with the aid of certified silicon solar cells without bias light. The stability tests were carried out under MPP under AM 1.5G one-sun illumination with a 420 nm long-pass UV-filter under N_2 environment. The cells were purged with nitrogen for 1 h before the MPP tracking.

Other Measurements: High-resolution scanning electron microscopy (SEM) images were obtained using field emission scanning electron microscope (FESEM, JEOL 7006F) with an accelerating voltage of 1 kV. The ultraviolet photoelectron spectroscopy (UPS) measurement was conducted on an AXIS ULTRA DLD (Kratos) Multitechnique system with photon source energy of 21.22 eV. Transmission electron microscopy (TEM) measurements were carried out on a high-resolution TEM (HR-TEM, JEM-2100) at an acceleration voltage of 200 kV. The EPR measurements were performed at room temperature using a Bruker EMX 10/12 spectrometer (Germany) with a computer for data acquisition and instrument control. Kelvin probe force microscope (KPFM) measurements were performed on a Bruker Dimension FastScan Scanning Probe Microscope (SPM). Light absorption properties were measured with ultraviolet-visible-inferred spectrophotometer (Varian Cary-5000). PL spectra were collected on HORIBA Jobin Yvon Fluorlog-3 system. TRPL spectroscopy measurements were conducted using a pulse laser (512 nm) for excitation (F980 lifetime spectrometers, Edinburgh Instruments, EI). The TRPL decays were recorded using a time-correlated single-photon counting (TCSPC) spectrometer. FTIR spectroscopy was performed on a Bruker Tensor spectrometer in transmission mode. The SPV spectrum were obtained from a measurement system containing the source of monochromatic light, a lock-in amplifier (SR830-DSP) with a light chopper (SR540). Electrochemical impedance spectra (EIS) were measured from a CHI 660E electrochemical workstation (Chenhua Inc., Shanghai), applying a 10 mV AC signal and scanning in a frequency range between 1 MHz and 1000 Hz at different forward applied bias. The crystal structure was researched by X-ray diffraction (XRD) on a Rigaku D/max-gA X-ray diffractometer with Cu K_α radiation ($\lambda = 1.5406$ Å).

Supporting Information

Supporting Information is available from the Wiley Online Library or from the author.

Acknowledgements

F.T. and M.I.S. contributed equally to this work. This publication is based in part on work supported by the National Key Research and Development Program of China (Grant No. 2017YFA0206600), by the

US Office of Naval Research (Grant Award No. N00014-17-1-2524), by the Ontario Research Fund Research Excellence Program, and by the Natural Sciences and Engineering Research Council (NSERC) of Canada. The work of F.T. was also supported by the China Scholarship Council (Grant No. 201608410244), the National Natural Science Foundation of China (Grant No. 61306019), the Natural Science Foundation of Henan Province (Grant no. 162300410026), the Key Member of Young Teachers (Grant no. 2016GGJS-019), and the Henan University Fund. H.T. acknowledges the Rubicon grant (680-50-1511) from the Netherlands Organisation for Scientific Research (NWO) and the National 1000 Young Talents award in China. M.I.S. acknowledges the support of the Banting Postdoctoral Fellowship Program, administered by the Government of Canada.

Conflict of Interest

The authors declare no conflict of interest.

Keywords

bilinkable ligands, charge recombination, contact interfaces, defect passivation, perovskite solar cells

Received: June 18, 2020
Published online:

[1] https://www.nrel.gov/pv/assets/images/best-research-cell-efficiencies.20190802.png.
[2] N. J. Jeon, H. Na, E. H. Jung, T.-Y. Yang, Y. G. Lee, G. Kim, H.-W. Shin, S. I. Seok, J. Lee, J. Seo, *Nat. Energy* **2018**, *3*, 682.
[3] J. A. Christians, P. Schulz, J. S. Tinkham, T. H. Schloemer, S. P. Harvey, B. J. Tremolet de Villers, A. Sellinger, J. J. Berry, J. M. Luther, *Nat. Energy* **2018**, *3*, 68.
[4] F. Li, J. Yuan, X. Ling, Y. Zhang, Y. Yang, S. H. Cheung, C. H. Y. Ho, X. Gao, W. Ma, *Adv. Funct. Mater.* **2018**, *28*, 1706377.
[5] X. Zhao, L. Tao, H. Li, W. Huang, P. Sun, J. Liu, S. Liu, Q. Sun, Z. Cui, L. Sun, Y. Shen, Y. Yang, M. Wang, *Nano Lett.* **2018**, *18*, 2442.
[6] E. Yalcin, M. Can, C. Rodriguez-Seco, E. Aktas, R. Pudi, W. Cambarau, S. Demic, E. Palomares, *Energy Environ. Sci.* **2019**, *12*, 230.
[7] H. Tan, A. Jain, O. Voznyy, X. Lan, F. P. Garc, R. Pudi, W. Cam, Z. Fan, R. Quintero-Bermudez, M. Yuan, B. Zhang, Y. Zhao, F. Fan, P. Li, L. N. Quan, Y. Zhao, Z.-H. Lu, Z. Yang, S. Hoogland, E. H. Sargent, *Science* **2017**, *355*, 722.
[8] L. Huang, X. Sun, C. Li, R. Xu, J. Xu, Y. Du, Y. Wu, J. Ni, H. Ca, J. Li, Z. Hu, J. Zhang, *Sol. Energy Mater. Sol. Cells* **2016**, *157*, 1038.
[9] S. You, H. Wang, S. Bi, J. Zhou, L. Qin, X. Qiu, Z. Zhao, Y. Xu, Y. Zhang, X. Shi, H. Zhou, Z. Tang, *Adv. Mater.* **2018**, *30*, 1706924.
[10] J.-Y. Seo, R. Uchida, H.-S. Kim, Y. Saygili, J. Luo, C. Moore, J. Kerrod, A. Wagstaff, M. Eklund, R. McIntyre, N. Pellet, S. M. Zakeeruddin, A. Hagfeldt, M. Grätzel, *Adv. Funct. Mater.* **2018**, *28*, 1705763.
[11] L. Zuo, Z. Gu, T. Ye, W. Fu, G. Wu, H. Li, H. Chen, *J. Am. Chem. Soc.* **2015**, *137*, 2674.
[12] L. Liu, A. Mei, T. Liu, P. Jiang, Y. Sheng, L. Zhang, H. Han, *J. Am. Chem. Soc.* **2015**, *137*, 1790.
[13] Q. An, P. Fassl, Y. J. Hofstetter, D. Becker-Koch, A. Bausch, P. E. Hopkinson, Y. Vaynzof, *Nano Energy* **2017**, *39*, 400.
[14] K. Wojciechowski, S. D. Stranks, A. Abate, G. Sadoughi, A. Sadhanala, N. Kopidakis, G. Rumbles, C.-Z. Li, R. H. Friend, A. K. Y. Jen, H. J. Snaith, *ACS Nano* **2014**, *8*, 12701.
[15] S. Chen, X. Zhang, J. Zhao, Y. Zhang, G. Kong, Q. Li, N. Li, Y. Yu, N. Xu, J. Zhang, K. Liu, Q. Zhao, J. Cao, J. Feng, X. Li, J. Qi, D. Yu, J. Li, P. Gao, *Nat. Commun.* **2018**, *9*, 4807.
[16] G. Divitini, S. Cacovich, F. Matteocci, L. Cin, Q. Di Carlo, C. Ducati, *Nat. Energy* **2016**, *1*, 15012.
[17] L. Liu, S. Huang, Y. Lu, P. Liu, Y. Zhao, C. Shi, S. Zhang, J. Wu, H. Zhong, M. Sui, H. Zhou, H. Jin, Y. Li, Q. Chen, *Adv. Mater.* **2018**, *30*, 1800544.
[18] S. Ye, H. Rao, Z. Zhao, L. Zhang, H. Bao, W. Sun, Y. Li, F. Gu, J. Wang, Z. Liu, Z. Bian, C. Huang, *J. Am. Chem. Soc.* **2017**, *139*, 7504.
[19] Q. Wang, C.-C. Chueh, T. Zhao, J. Cheng, M. Eslamian, W. C. H. Choy, A. K.-Y. Jen, *ChemSusChem* **2017**, *10*, 3794.
[20] J. Wang, K. Datta, C. H. L. Weijtens, M. M. Wienk, R. A. J. Janssen, *Adv. Funct. Mater.* **2019**, *29*, 1905883.
[21] H. Sun, K. Deng, Y. Zhu, M. Liao, J. Xiong, Y. Li, L. Li, *Adv. Mater.* **2018**, *30*, 1801935.
[22] K. Mahmood, B. S. Swain, A. Amassian, *Adv. Energy Mater.* **2015**, *5*, 1500568.
[23] M. Schmidt, G. S. Samuel, *Fresenius' J. Anal. Chem.* **1991**, *341*, 412.
[24] J. Schnadt, J. N. O. Shea, L. Patthey, J. Schiessling, J. Krempaskn, . K.-Y. Jen, Z. Bian, C. Huang, Y. Li, *Surf. Sci.* **2003**, *544*, 74.
[25] P. Meriaudeau, O. H. Ellestad, M. Dufaux, *J. Catal.* **1982**, *75*, 243.
[26] S. Wu, X. Liu, X. Lian, G. Tian, C. Janiak, Y. Zhang, Y. Lu, H. Yu, J. Hu, H. Wei, H. Zhao, G. Chang, G. V. Tendeloo, L. Wang, X. Yang, B. Su, *Adv. Mater.* **2018**, *30*, 1802173.
[27] L. Kronik, Y. Shapira, *Surf. Sci. Rep.* **1999**, *37*, 1.
[28] M. Li, X. Yan, Z. Kang, X. Liao, Y. Li, X. Zheng, P. Lin, J. Meng, Y. Zhang, *ACS Appl. Mater. Interfaces* **2017**, *9*, 7224.
[29] Y. H. Lin, D. J. Wang, Q. D. Zhao, M. Yang, Q. L. Zhang, *J. Phys. Chem. B* **2004**, *108*, 3202.
[30] L. Jing, S. Li, S. Song, L. Xue, H. Fu, *Sol. Energy Mater. Sol. Cells* **2008**, *92*, 1030.
[31] D. Bi, C. Yi, J. Luo1, J.-D. Décoppet, F. Zhang, S. M. Zakeeruddin, X. Li, A. Hagfeldt, M. Grätzel, *Nat. Energy* **2016**,*1*, 142.
[32] W. Zhang, S. Pathak, N. Sakai, T. Stergiopoulos, P. K. Nayak, N. K. Noel, A. A. Haghighirad, V. M. Burlakov, D. W. deQuilettes, A. Sadhanala, W. Li, L. Wang, D. S. Ginger, R. H. Friend, H. J. Snaith, *Nat. Commun.* **2015**, *6*, 10030.
[33] Y. Liu, K. Palotas, X. Yuan, T. Hou, H. Lin, Y. Li, S.-T. Lee, *ACS Nano* **2017**, *11*, 2060.
[34] N. Zhao, T. P. Osedach, L.-Y. Chang, S. M. Geyer, D. Wanger, M. T. Binda, A. C. Arango, M. G. Bawendi, V. Bulovic, *ACS Nano* **2010**, *4*, 3743.
[35] K. Jiang, J. Wang, F. Wu, Q. Xue, Q. Yao, J. Zhang, Y. Chen, G. Zhang, Z. Zhu, H. Yan, L. Zhu, H.-L. Yip, *Adv. Mater.* **2020**, *32*, 1908011.
[36] B. Sun, O. Voznyy, H. Tan, P. Stadler, M. Liu, G. Walters, A. H. Proppe, M. Liu, J. Fan, T. Zhuang, J. Li, M. Wei, J. Xu, Y. Kim, S. Hoogland, E. H. Sargent, *Adv. Mater.* **2017**, *29*, 1700749.
[37] Z. Ning, O. Voznyy, J. Pan, S. Hoogland, V. Adinolfi, J. Xu, M. Li, A. R. Kirmani, J.-P. Sun, J. Minor, K. W. Kemp, H. Dong, L. Rollny, A. Labelle, G. Carey, B. Sutherland, I. Hill, A. Amassian, H. Liu, J. Tang, O. M. Bakr, E. H. Sargent, *Nat. Mater.* **2014**, *13*, 822.
[38] J. Chen, X. Zhao, S.-G. Kim, N.-G. Park, *Adv. Mater.* **2019**, *31*, 1902902.
[39] Q. Jiang, Y. Zhao, X. Zhang, X. Yang, Y. Chen, Z. Chu, Q. Ye, X. Li, Z. Yin, J. You, *Nat. Photonics* **2019**, *13*, 460.
[40] R. Calarco, M. Marso, T. Richter, A. I. Aykanat, R. Meijers, A. V. D. Hart, T. Stoica, H. Lüth, *Nano Lett.* **2005**, *5*, 981.
[41] W. K. Hong, G. Jo, S. S. Kwon, S. Song, T. Lee, *IEEE Trans. Electron Devices* **2008**, *55*, 3020.
[42] C.-Y. Chen, J. Ramon, D. Retamal, I.-W. Wu, D.-H. Lien, M.-W. Chen, Y. Ding, Y.-L. Chueh, C.-I. Wu, J.-H. He, *ACS Nano* **2012**, *6*, 9366.
[43] M. Hannula, H. Ali-L€oytty, K. Lahtonen, J. Saari, A. Tukiainen, M. Valden, *Acta Mater.* **2019**, *174*, 237.
[44] W. Kong, W. Li, C. Liu, H. Liu, J. Miao, W. Wang, S. Chen, M. Hu, D. Li, A. Amini, S. Yang, J. Wang, B. Xu, C. Cheng, *ACS Nano* **2019**, *13*, 4049.

[45] D. Yang, X. Zhang, K. Wang, C. Wu, R. Yang, Y. Hou, Y. Jiang, S. Liu, S. Priya, *Nano Lett.* **2019**, *19*, 3313.
[46] Q. Jiang, Z. Chu, P. Wang, X. Yang, H. Liu, Y. Wang, Z. Yin, J. Wu, X. Zhang, J. You, *Adv. Mater.* **2017**, *29*, 1703852.
[47] Y. Zhao, H. Tan, H. Yuan, Z. Yang, J. Z. Fan, J. Kim, O. Voznyy, X. Gong, L. N. Quan, C. S. Tan, J. Hofkens, D. Yu, Q. Zhao, E. H. Sargent, *Nat. Commun.* **2018**, *9*, 1607.
[48] T. Leijtens, G. E. Eperon, S. Pathak, A. Abate, M. M. Lee, H. J. Snaith, *Nat. Commun.* **2013**, *4*, 2885.
[49] W. Li, W. Zhang, S. V. Reenen, R. J. Sutton, J. Fan, A. A. Haghighirad, M. B. Johnston, L. Wang, H. J. Snaith, *Energy Environ. Sci.* **2016**, *9*, 490.
[50] Y. Du, H. Cai, Y. Wu, Z. Xing, Z. Li, J. Xu, L. Huang, J. Ni, J. Li, J. Zhang, *Phys. Chem. Chem. Phys.* **2017**, *19*, 13679.
[51] J. Christians, R. Fung, R. Kamat, *J. Am. Chem. Soc.* **2014**, *136*, 758.
[52] J. Jung, C. Chueh, A. Jen, *Adv. Mater.* **2015**, *27*, 7874.
[53] Y. Chen, N. Li, L. Wang, L. Li, Z. Xu, H. Jiao, P. Liu, C. Zhu, H. Zai, M. Sun, W. Zou, S. Zhang, G. Xing, X. Liu, J. Wang, D. Li, B. Huang, Q. Chen, H. Zhou, *Nat. Commun.* **2019**, *10*, 1112.
[54] S. Ye, H. Rao, W. Yan, Y. Li, W. Sun, H. Peng, Z. Liu, Z. Bian, Y. Li, C. Huang, *Adv. Mater.* **2016**, *28*, 9648.
[55] F. Tan, Z. Wang, S. Qu, D. Cao, K. Liu, Q. Jiang, Y. Yang, S. Pang, W. Zhang, Y. Lei, Z. Wang, *Nanoscale* **2016**, *8*, 10198.